Controlled Synthesis of Pt doped Nanotitania as Visible Light Responsive Photocatalyst

Suprabha.T[1], Suresh Mathew[2]

[1]SreeNarayanaGurukulam College of Engineering, Kadayiruppu, Ernakulam,India682 311
[2]Advanced Molecular Materials Research Centre, Mahatma Gandhi University,
Kottayam, India 686 560

Abstract: *Nanotitania with three different morphologies viz., cubes, spheres and rods were synthesized by microwave irradiation. Nano-sized platinum particles were doped on nanotitania by metal sol method under controlled conditions. Photocatalytic degradation of methylene blue over bare and platinum doped titania was conducted under sunlight to investigate the effect of Pt on the dye degradation property of nanotitania As-synthesized TiO_2 and Pt-TiO_2 nanostructures were characterized by X-ray diffraction (XRD), UV-visible spectroscopy, Raman spectroscopy, BET surface area, Photoluminescence (PL), Field emission scanning electron microscopy (FESEM) with EDX, Transmission electron microscopy (TEM) and Atomic force microscopy (AFM) techniques.. The dye degradation capabilities of nano-sized Pt-TiO_2 catalysts were found superior to bare TiO_2 nanostructures. The higher photoactivity of Pt-TiO_2 can be ascribed to the effect of platinum deposits acting as electron traps on the Pt-TiO_2 surface. Optical characterization by UV-visible spectrophotometer showed a shift in absorption wavelength to the visible region due to the incorporation of platinum nanoparticles into nanotitania.*

Keywords: dye degradation, microwave synthesis, nanotitania, photocatalysis, Pt/ TiO_2

I.   Introduction

Microwave synthesis and photocatalysis are important chapters of green chemistry [1-7]. Alternative energy sources (e.g., microwaves, solar) and their combination can be used for the development of greener synthetic methods for a wide range of applications that are not only restricted to catalysis but also include a variety of applications related to medicine, the environment and nanoscience [8-12]. In this sense, the search for environmentally benign, sustainable, and efficiently reusable alternative catalytic systems has become critical.

Nowadays, there is a great concern to guarantee the future sources and settle securely the provision of clean drinking water, soil and air. Photocatalytic oxidation has recently applied to remove atmospheric NO*x*, which is believed to cause acid rain and to be toxic to human health. Titanium dioxide (TiO_2) photocatalyst is found to be able to oxidize low-level NO*x* (near 1 ppm or below) in air to HNO3 very rapidly [13,14]. It has been commonly accepted that titanium dioxide (TiO_2) is one of the most popular photocatalysts among the semiconductors. It is environmentally benign and relatively inexpensive with unique electronic and optical properties and has the distinct advantages such as low operation temperature, ease of availability, non-toxicity, high photocatalytic activity, ease of handling and high resistance to photo-induced decomposition. It also exhibits long-term stability against photo and chemical corrosion.

As a most widely used photocatalyst, TiO_2 has a relatively large band gap of 3.2 eV, corresponding to wavelengths of shorter than 388 nm. Restated, TiO_2 can use only 3-4% of the solar energy that reaches the earth [15]. The general approach is to modify TiO_2 by creating intra-band gap states that are close to the conduction or valence band edges, and absorb visible light at sub-band gap energies of less than 3.2 eV [16]. For the purpose of overcoming these limitations of TiO_2 as a photocatalyst, numerous studies have been performed to enhance electron–hole separation and to extend the absorption range of TiO_2 into the visible range. These studies include doping metal ions into the TiO_2 lattice, dye photosensitization on the TiO_2 surface, addition of inert support and deposition of noble metals [17-23]. However, the efficiency of TiO_2-based photocatalysts directly depends on the ability to obtain nanostructured materials with tailored features to generate electron–hole pairs with a reduced recombination rate and to reduce the energy band gap sufficiently to absorb visible light [15, 16].

We have already reported a simple microwave method to synthesize phase pure anatase and rutile nanotitania with different morphologies viz., cubes, spheres and rods [24]. In an attempt to modify the optical properties of titania synthesized by microwave irradiation we were successful in loading Au, Ag and Pd into titania structures which shifted the absorption into visible region [25, 26, 27]. In the present work, we could

enhance the visible light photocatalysis of nanotitania by loading platinum by metal sol method [28]. To the best of our knowledge no reports are available with regard to the preparation of Pt doped TiO_2 using TiO_2 synthesized by microwave irradiation. Microwave reactions attain high temperature rapidly and do not require long time for completion. Shorter reactions are advantageous, as they save time and are more economical and facilitate the synthesis of metastable compounds, which are difficult to synthesize otherwise. Metal sol method was reported [28] for the preparation of supported gold catalysts via 'size-controlled' gold colloids. In this study, metal sol method was employed for the preparation of platinum doped nanotitania for enhanced photocatalysis. The catalytic performances of three morphologically different nanotitania and their platinum doped nanostructures (Pt-TiO_2) were studied for dye degradation of methylene blue under sunlight.

II.   Experimental

2.1. Materials

All reagents were purchased from Merck, Germany. Titanium trichloride (15 wt. % $TiCl_3$, 10 wt. % HC1) was used as the titanium precursor. NH_4OH (1.5 M), NaCl (5 M), NH_4Cl (5 M), hexachloroplatinic acid (H2PtCl6), $NaBH_4$, and polyvinyl alcohol (PVA) were employed for the synthesis. A typical microwave oven (Whirlpool, 1200 W) operating at a frequency of 2450 MHz was used for the synthesis.

2.2. Synthesis of Pt doped TiO_2 nanostructures

The three TiO_2 nanostructures with different morphologies viz., cube, sphere and rod (S1, S2, S3) synthesized as per our early report [25], were doped with 1 wt% Pt employing metal sol method. For this a suitable amount of PVA solution (1wt %) was added to an aqueous hexachloroplatinic acid solution (0.1 mg Pt/ml) under vigorous stirring. Then, a freshly prepared solution of $NaBH_4$ (molar ratio $NaBH_4$/ Pt = 4) was slowly added dropwise into the mixture. The TiO_2 samples were added after the pH of Pt sol was adjusted to 6.0 by NH_4OH or HCl solution. The mixture was stirred at 60^0C for 3 hrs, then filtered and washed until no Cl^- was detected by $AgNO_3$ solution. After being dried at $100^0 C$ overnight, the samples were calcined at 550^0C in air for 4 hrs. The platinum doped on samples S1, S2 and S3 are represented as PtS1, PtS2 and PtS3 respectively.

2.3. Characterization of Nanotitania

The X-ray diffraction (XRD) patterns of the titania were recorded on a Brucker D8 advance diffractometer with CuKα radiation. The crystallite size of TiO_2 was calculated using Debye Scherrer equation, $L = k\lambda/(ß \cos\theta)$, where L is the average crystallite size, λ is the wavelength of the radiation, θ is the Bragg's angle of diffraction, ß is the full width at half maximum intensity of the peak and k is a constant usually applied as 0.89. A Jeol JSM 6500F scanning electron microscope was used for FESEM studies. High resolution transmission electron micrographs and electron diffraction patterns were recorded using a JEOL JEM-3010 HRTEM microscope at an accelerating voltage of 300 kV. The TEM specimens were prepared by drop casting the sample on the surface of carbon coated copper grid. The tapping mode AFM images of the samples deposited on a mica sheet were taken using Nanoscope-IV scanning probe microscope. The BET surface area, pore size distribution and pore volume of the samples were measured on a Micromeritics ASAP 2010 analyzer based on N_2 adsorption at 77 K in the pressure range from 0.1 to 760 mmHg. The ultraviolet–visible absorption (UV–vis) spectra were recorded using a UV-2450 Shimadzu UV–visible spectrophotometer. The photoluminescence (PL) spectral measurements were made using Perkin Elmer LS-55 luminescence spectrometer at an excitation wavelength of 325 nm. Raman spectroscopic analysis was done using a Horiba Jobi Voyan Mof i-550 spectrophotometer.

2.4. Photocatalytic Activity Measurements

Photocatalytic activity of TiO_2 was evaluated by the degradation of the dye, methylene blue (MB) in aqueous solution under sunlight in the presence of as-synthesized TiO_2 and the Pt doped TiO_2 nanostructures. The changes in the concentrations of methylene blue in the aqueous solution were examined by absorption spectra measured on a UV-2450 Shimadzu UV–visible spectrophotometer. Before examining the photocatalytic activity for the degradation of aqueous methylene blue, TiO_2 and Pt-TiO_2 sol was prepared. About 100 mg of the synthesized TiO_2 or Pt-TiO_2 was dispersed ultrasonically in 100 ml of $4 \times 10^{-5}M$ methylene blue solution in a quartz reactor. To maximize the adsorption of the dye onto the TiO_2 surface, the resulting mixture was kept in the dark for 30 min under stirring conditions [29]. The solution was then irradiated by exposing to sunlight for three hours, viz.., from 11-14 hrs during the month of February when the sunlight with bright and constant

intensity was abundantly available. We have checked the intensity of the sunlight using YSI 9500 Photometer (1.413 kW/m^2) and was found quite uniform during the month of February, when the experiments were done. The degradation of the dye was monitored by measuring the absorption maximum of methylene blue at 661 nm at 30 min intervals of reaction.

III.   Results and Discussion

3. 1. X-ray Diffraction Studies

The X-ray diffraction (XRD) pattern (Fig. 1) shows that anatase TiO$_2$ phase with lattice constants, a = 3.777 and c = 9.501 was formed (JCPDS file no. 89-4921) when NH$_4$OH was used as the medium (S1). All the diffraction peaks of nanotitania synthesized in NaCl medium (S2) and NH$_4$Cl medium (S3) correspond to rutile phase with lattice constants a = 4.608, c = 2.973 and a = 4.548, c = 2.946, respectively (JCPDS files, no. 76-0319 and 88-1173). It is clear from the X-ray diffractograms that all the samples are highly crystalline. There is no phase change for the nanotitania after platinum loading on the samples S1, S2 and S3
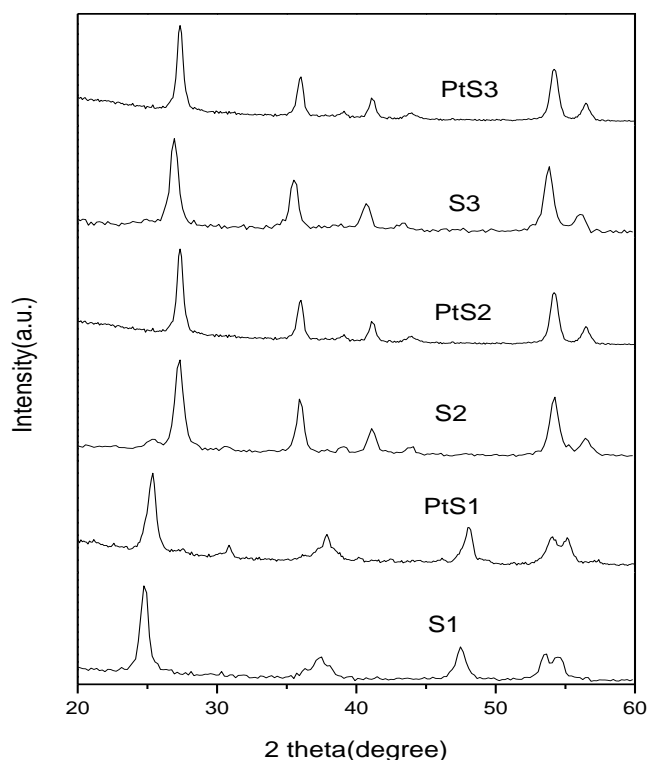

Figure 1. XRD patterns of bare and platinum doped nanotitania

Further, no platinum peaks were found in the XRD patterns and may be due to the low platinum content in these nanotitania. The average crystallite sizes of S1, S2, S3, PtS1, PtS2 and Pt S3 are 12, 10, 21, 11, 9 and 19 nm respectively which shows that there is only little effect on the crystallite size of TiO$_2$ nanoparticles on platinum loading. The X-ray diffraction patterns of platinum doped TiO$_2$ samples almost coincide with that of bare TiO$_2$ indicating that the metal sol method yields highly dispersed pt particles on the TiO$_2$ photocatalyst [30, 31].

Table 1 The crystallite size, BET surface area, pore size and pore volume values of bare and Pt doped TiO_2 samples

Sample code	Crystallite Size (nm)	BET surface area ($m^2 g^{-1}$)	Pore size (nm)	Pore volume ($cm^3 g^{-1}$)
S1	12	96	4	0.37
S2	10	77	2.5	0.18
S3	21	34	2.0	0.10
Pt S1	11	91	2.4	0.28
PtS2	9	72	1.8	0.11
Pt S3	19	30	1.4	0.09

3.2. BET Surface Area Analysis

The crystallite size, BET surface area, pore size and pore volume values are summarized in Table 1. The surface area of S1, S2 and S3 are 96, 77 and 34 $m^2 g^{-1}$, respectively. The sample S1 has highest surface area and is due to its mesoporous nature with pore size around 4 nm. platinum doped TiO_2 particles show a decrease in surface area of the samples S1, S2 and S3 as is evident from the table 1 The platinum nanoparticles inserted into the pores of mesoporous titania, reduced its surface area. However, this reduction is not detrimental to its photocatalytic activity. The platinum on the nanotitania surface act as a sink for electron capture and enhanced the photo catalysis by prolonging the lifetime of photogenerated electron-hole pairs. In spite of its low surface area, platinum doped nanotitania exhibits well crystalline phases which are able to degrade the methylene blue reasonably. The pore volume of the platinum doped nanotitania is comparatively less than that of nanotitania. This trend is consistent with surface area and pore size results [32].
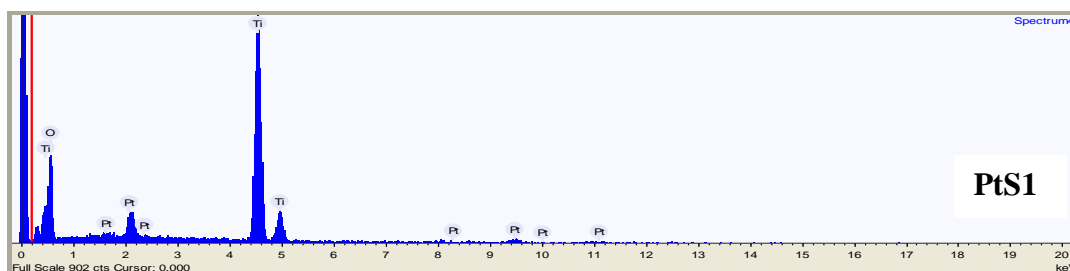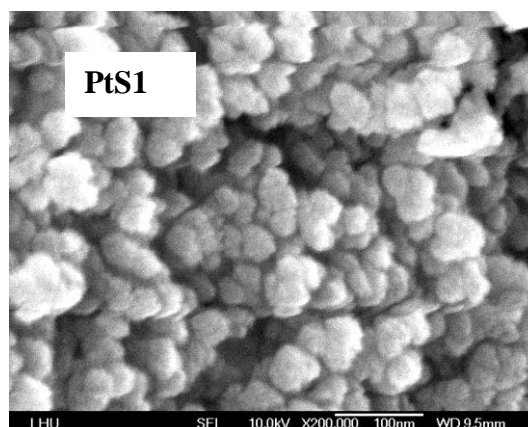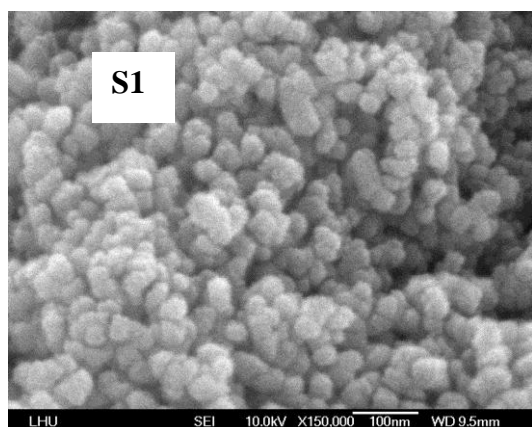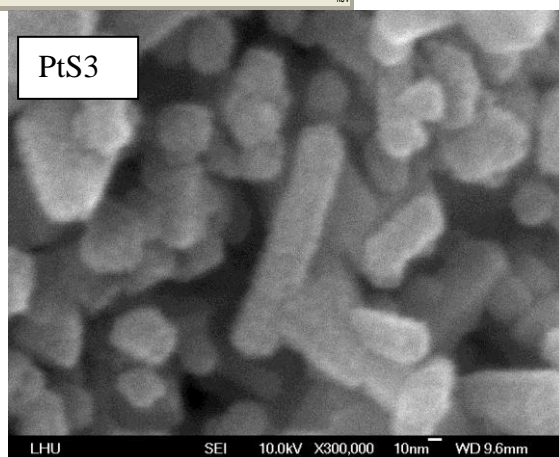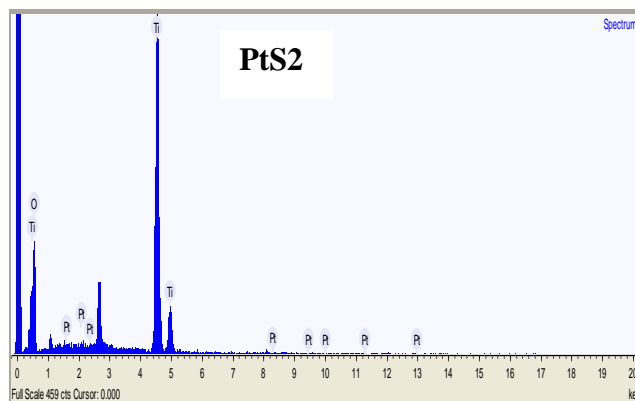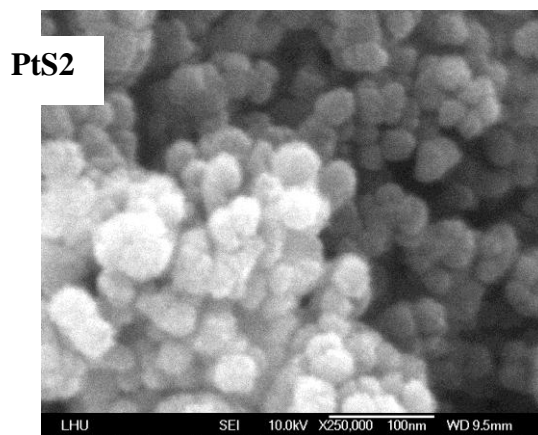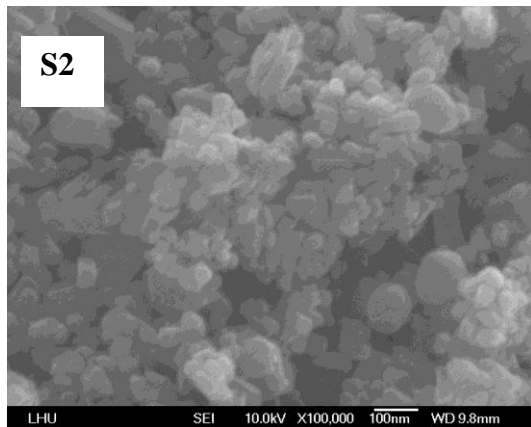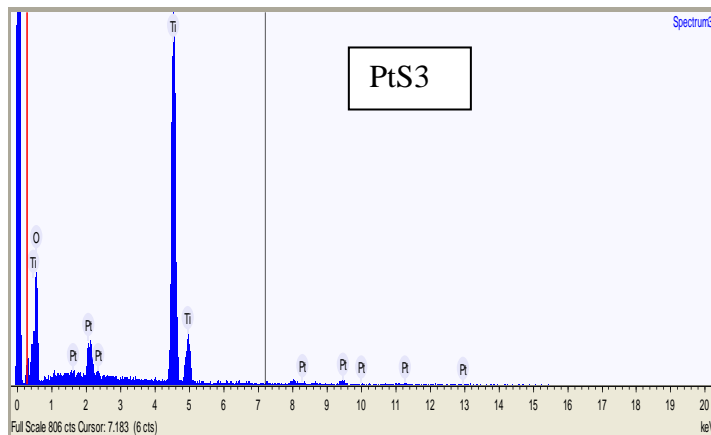
Figure 2. FESEM of bare and Pt doped titania and EDX of Pt doped nanotitania

3.3. Electron Microscopic Analysis

FESEM images of bare and platinum doped titania samples are given in Fig. 2. S1, S2 and S3 show a cube-like morphology, spherical morphology and rod-like morphology, respectively. The elemental analyses of the samples were done by energy dispersive X-ray spectroscopy (EDX) experiments, which were carried out in the FESEM. The presence of 1wt % platinum was confirmed from EDX analysis for all the three samples (PtS1, PtS2 and Pt S3) (Fig. 2). Different concentrations of platinum in all the three samples were tried but optimum results were obtained with 1wt% Pt.
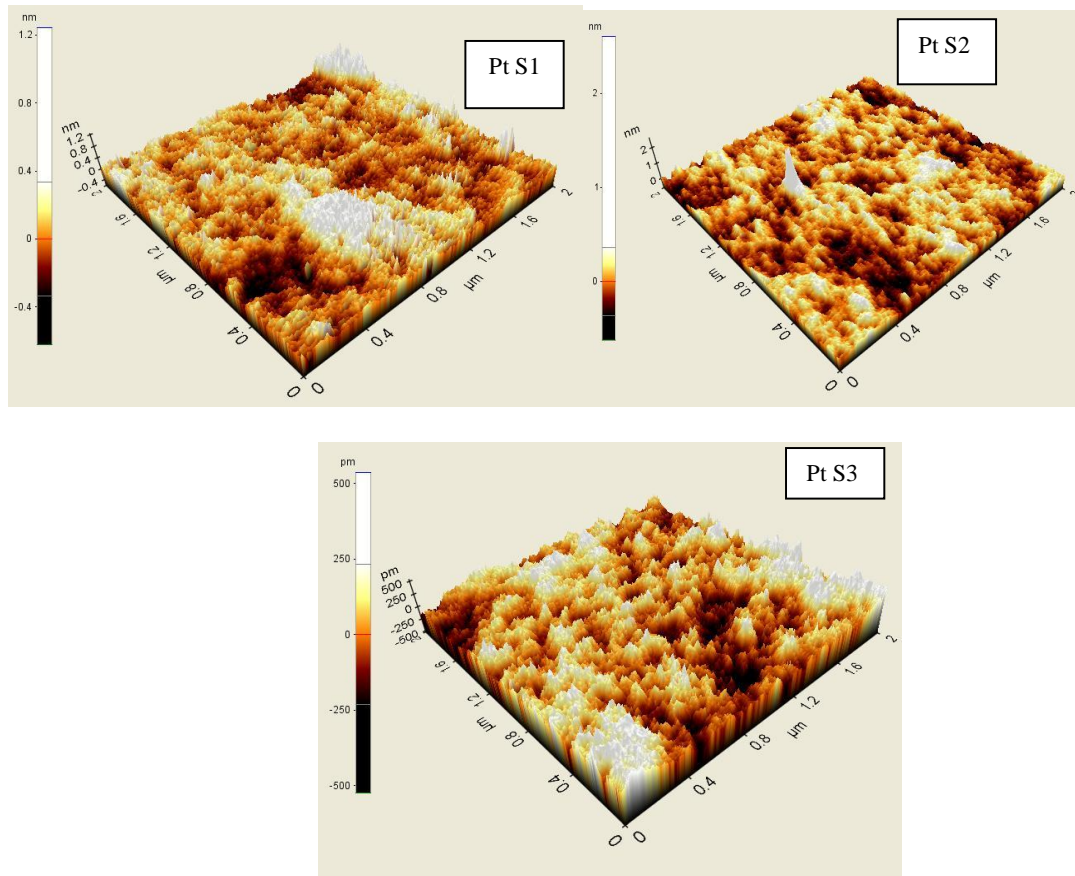

Figure 3. AFM images of the Pt doped titania

Fig. 3 represents AFM images of platinum doped TiO_2 samples. platinum particles are not seen in FESEM images or AFM images and may be due to its small size.

The high resolution TEM images of the bare and platinum doped TiO_2 nanoparticles synthesized are shown in Fig. 4. TEM image of S1 (a) shows the formation of nanocubes with particle size around 25 nm with pores. The HRTEM image S1 (b) shows lattice fringes of the anatase phase with d = 0.34 nm. Due to high symmetry in cubic morphology, lattice points are perfectly packed leading to the single crystalline nature which is evident from selected area electron diffraction pattern. As the surface energy of nano cube is high, there is a tendency to agglomerate which is clear from HRTEM results. The high surface area observed for the sample S1 may be due to the highly porous nature of the cubes. Since the sample S1 is not an ordered mesoporous system, pores cannot be viewed clearly from HRTEM images. Sample S2 (c) shows the formation of nanospheres of average particle size around 8 nm. Corresponding selected area electron diffraction pattern is shown in the inset. The pattern indicates the polycrystalline nature of the sample. Lattice image S2 (d) of these nanospheres shows lattice fringes of the rutile phase with d = 0.32 nm. Sample S3 (e) shows the formation of nanorods with an average aspect ratio of around 4 nm. Corresponding SAED pattern indicates a polycrystalline nature, which may be due to the diffraction in a bunch of nanorods. The HRTEM image S3 (f) of the rutile nanorods show clear lattice fringes of the rutile phase with d = 0.32 nm. Pt doped samples showed the presence of very small and well dispersed platinum nanoparticles on the TiO_2 surface and it appears as black spots in Fig. 4 (PtS1, PtS2 and PtS3). The platinum particles seen in the TEM images are comparatively less. This may be attributed to the low platinum content in the TiO_2 samples.
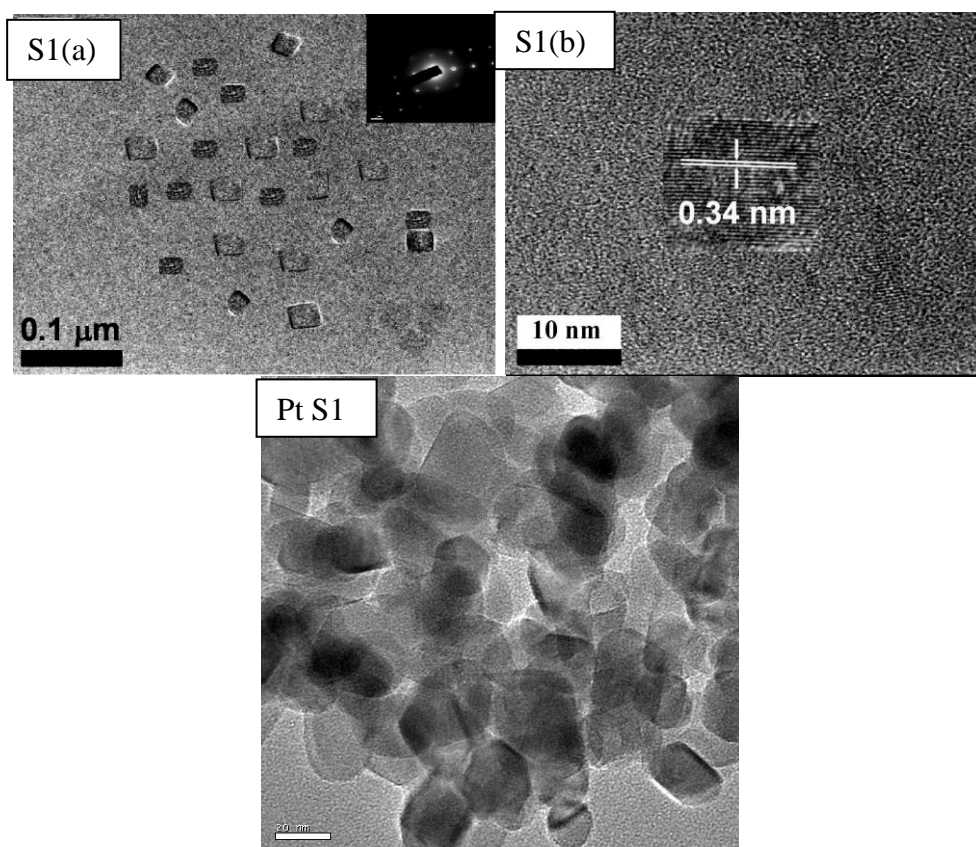

Fig. 4. HRTEM images of: (a) S1 (nanocubes) and (b) corresponding lattice
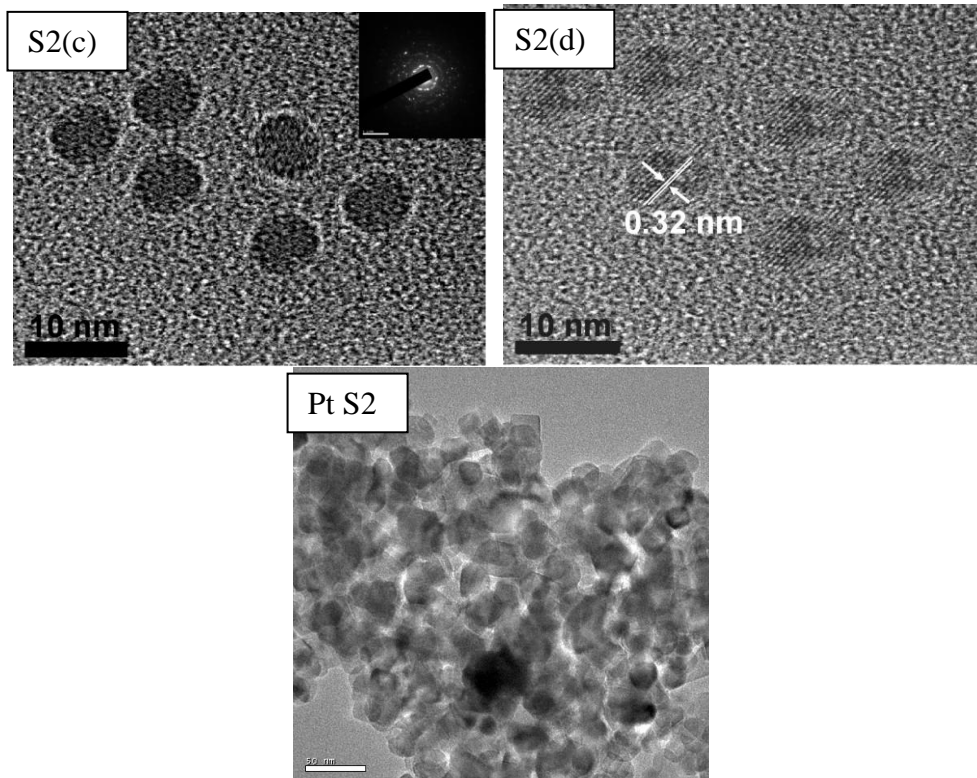
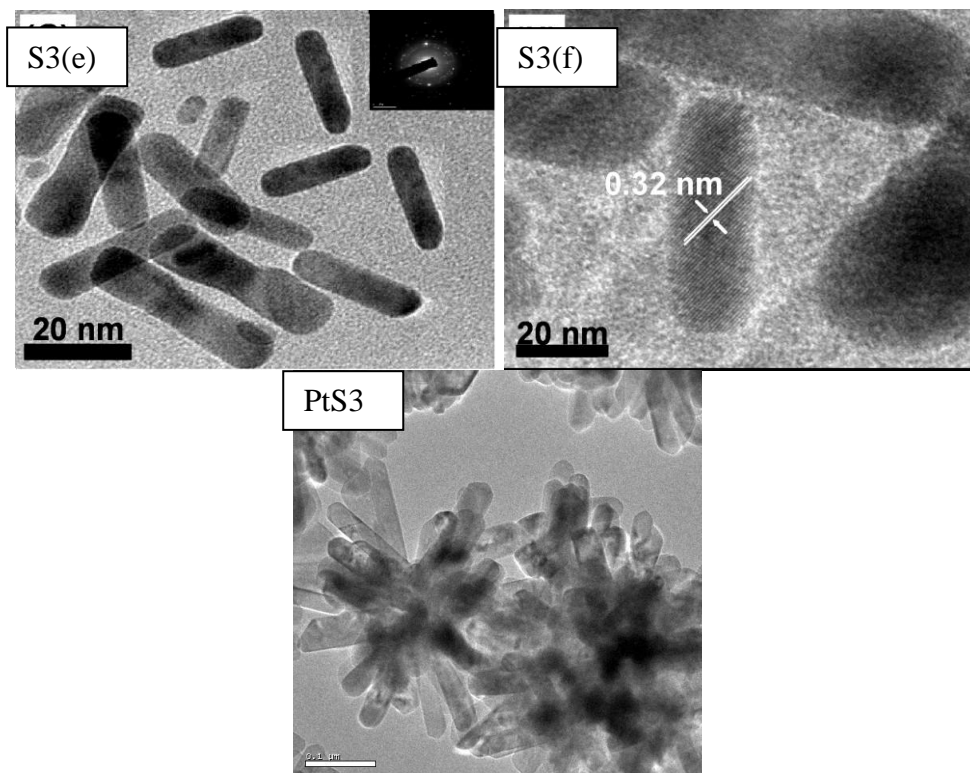**Fig. 4.** HRTEM images of: (a) S2 (nano spheres) and (b) corresponding lattice;

Fig. 4. HRTEM images of: (a) S3 (nano rods) and (b) corresponding lattice;

3.4. UV–visible Absorption Studies

Fig. 5 shows the UV-vis absorption spectra of nanotitania S1, S2, and S3. The onset of absorption for the three samples is 382, 405 and 415 nm for S1, S2 and S3, respectively. It is clear from the fig. 5 that platinum doped samples showed significant absorption in the visible region. The red shifted photo response of these samples may lead to high photocatalytic activity under visible region which helps in the enhancement of photocatalytic activity under sunlight. As for Pt doped nanotitania, the surface plasmon resonance (SPR) peak is absent because Pt nano particles have no characteristic peak in the region of 300-800 nm[33]. The band gap energies were calculated by the equation;

$$Eg = 1239.8/\lambda$$

where Eg is the band gap (eV) and λ (nm) is the wavelength of the absorption edges in the spectrum. The band gap values of platinum doped and bare TiO_2 samples are given in Table 2. The band gap of nanocubes (S1, 3.2 eV) is significantly higher compared to that of nanospheres (S2, 3.17 eV) and nanorods (S3, 3.15 eV). The band gap (Eg) of S1 is estimated to be 3.2 eV, which is in good agreement with the reported value for anatase (3.2–3.3 eV). However, rutile nanostructures show a slightly higher band gap than the reported value (3.0–3.1 eV). The higher band gap may be due to the smaller particle size. The band gap values of platinum doped TiO_2 samples are less than that of bare nanoTiO_2 samples. The lower band gap of platinum doped TiO_2 can enhance the photo catalytic activity of these samples under visible light.
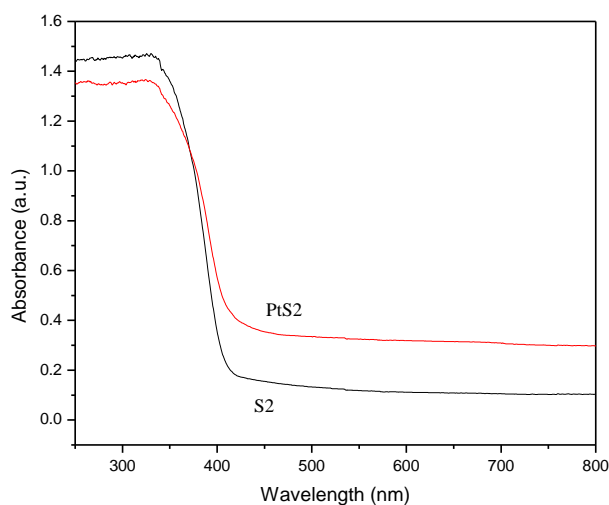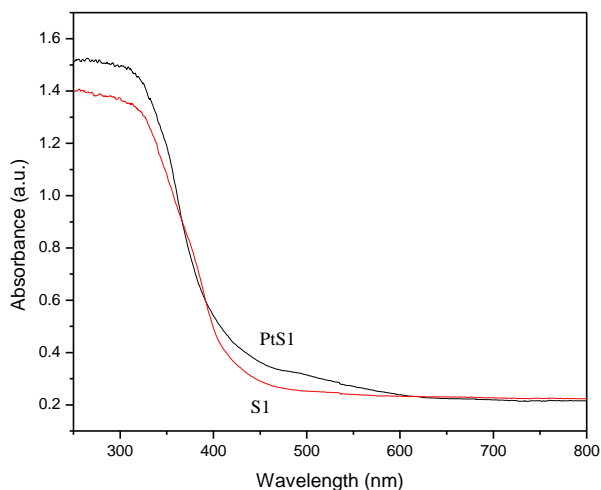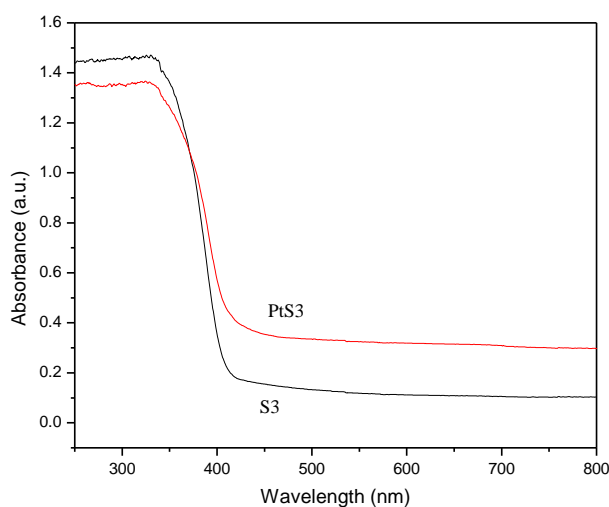
Figure 5. UV–visible absorption spectra of bare and platinum doped TiO_2 samples

3.5. Photoluminescence Studies

The photoluminescence emission spectra (PL) of Pt doped and bare TiO_2 samples were studied in the range of 250-700 nm to investigate the separation efficiency of charge carriers and the results are shown in Fig. 6.

It is evident from the figure that the PL intensity of TiO_2 was decreased with Pt doping. The PL intensity reflects the recombination possibility of electrons and holes. As the PL intensity decreased with Pt doping, we can infer that the feasibility of recombination of photoexcited electrons and holes is low [20, 21]. The electrons are excited from valence band (VB) to conduction band (CB) of TiO_2 under irradiation and generate photoexcited electrons and holes. Although loading with Pt narrows the band gap of TiO_2 samples, the recombination of electrons and holes are relatively slow which is evident from PL spectra. The plausible explanation for this observation is that Pt doped on the surface may also block part of the excitation light and the emission light [21].

Table 2 Band gap values of bare and Pt doped TiO_2 samples

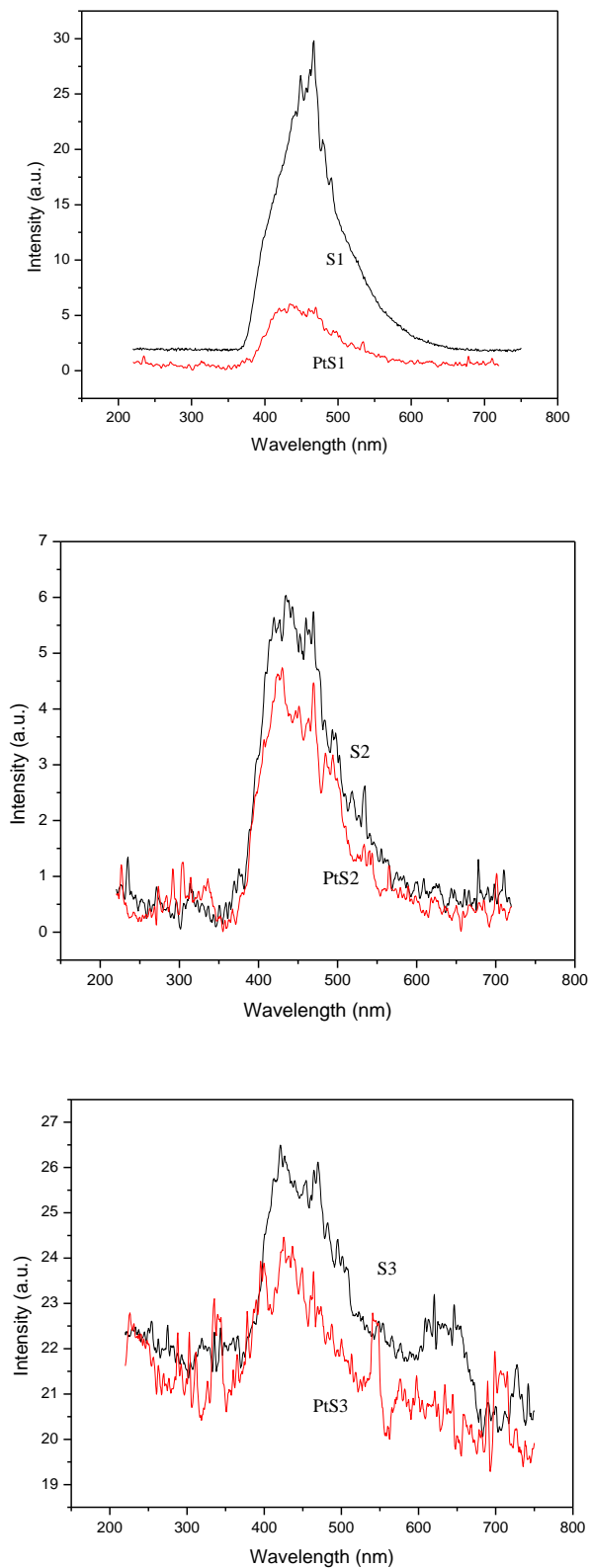| Sample	Band gap (eV)
S1	3.2
S2	3.17
S3	3.15
PtS1	2.91
PtS2	2.84
PtS3	2.87

Figure 6. The photoluminescence (PL) emission spectra of bare and Pt doped TiO_2 samples

For Pt doped TiO_2 samples, Pt plays an important role in the interfacial charge transfer and in the decrease in rate of electron-hole recombination. Pt particles could act as an effective electron scavenger to trap the photo induced electrons and holes of TiO_2 leading to the reduction of electron–hole recombination and thus improving the photocatalytic efficiency[34]. The decrease in PL intensity of Pt doped samples are in the order PtS1>PtS2>PtS3 as evident from the figures which indicate that the electron – hole recombination is less for PtS1 than PtS2 and PtS3. This low electron – hole recombination result in the higher photocatalytic activity of PtS1 than PtS2 which in turn is greater than PtS3. The electrons trapped in Pt sites were subsequently transferred to the surrounding adsorbed O_2. The PL spectrum is used to investigate the fate of electron hole pairs in semiconductor particles since PL emission results from the recombination of free carriers [20, 34].

3.6. Raman Spectral Studies

Raman spectroscopy is a powerful technique for the investigation of various phases of TiO_2 because it is capable of elucidating the structure as peaks from each material which are clearly separated in frequency and therefore, the phases are easily distinguishable[35, 36]. The expected vibrational modes of anatase TiO_2 are $A_1g + 2B_1g + 3Eg$ at 147, 197, 396, 515 and 638 cm^{-1}, and that of rutile are, $A_1g + B_1g + B_2g + Eg$ at 144, 238, 447 and 611 cm^{-1} [11, 44, 45]. Fig. 7 (a, b and c) shows the Raman scattering patterns of bare and Pt doped TiO_2 powders. The Raman spectra of bare nanotitania (S1) in Fig. 7 a shows that the anatase is the predominant phase, which is in accordance with the XRD analysis. It is found that the spectra of bare and Pt doped titania nanocube are similar. Both spectra show four Raman bands associated with the TiO_2 at around 146, 401, 514 and 638 cm^{-1}[37]. The Raman peaks at 146 and 638 cm^{-1} are assigned to the Eg modes of anatase phase and the Raman peak at 401 cm^{-1} is assigned to the B_1g mode. The peak at 514 cm^{-1} is a doublet of the A_1g and B_1g modes of anatase phase [38]. Raman peaks at $238(B_{2g})$, $447(E_g)$ and $611(A_{1g})$ cm^{-1} of spherical nanotitania (S2 and PtS2) and $446(E_g)$ and $612(A_{1g})$ cm^{-1} of rod shaped nanotitania (S3 and PtS3) are assigned to rutile phase (Fig. 7 b and c) which are in accordance with the XRD analysis. In the case of rutile nanosphere, the intensity of the peak at144 cm^{-1} (B_1g) is behaving in a different manner, after Pt doping. The decrease in intensity of this lowest frequency mode may be assigned to the spherical morphology of rutile nanotitania.
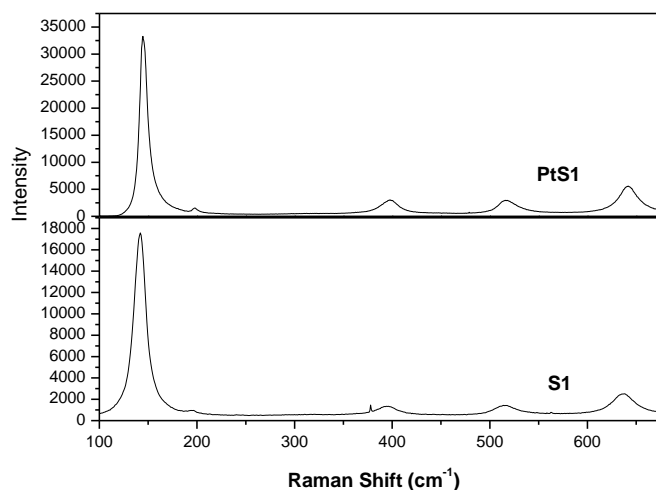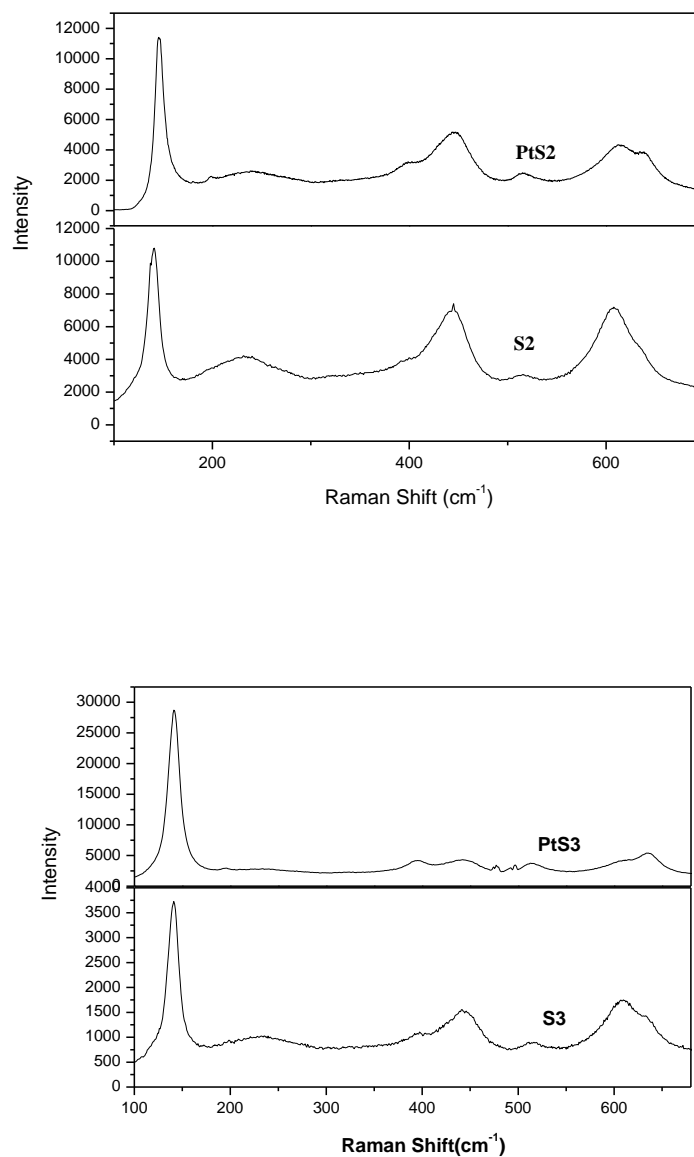
Figure 7. Raman spectra of bare and Pt doped TiO_2 samples

The Pt doped TiO_2 powder shows much stronger vibration peaks due to the surface enhanced Raman scattering effect (SERS) [39,40]. The SERS effect includes electromagnetic and chemical enhancement. No electromagnetic field block between doped Pt and TiO_2 can lead to the coupling of their electromagnetic fields. Since the 512 nm Ar^+ laser line is in the region of the plasmon absorption of Pt particles, the electrons located at Pt particle surface could be excited to high energy states. Those electrons can couple with the laser light, leading to an obvious resonance and strong localized fields. As a result, the Pt doped TiO_2 powder shows enhanced Raman scattering, indicating that Pt particles are tightly connected with TiO_2 grains. Raman intensities of spectral lines increases on Pt loading [36, 41].
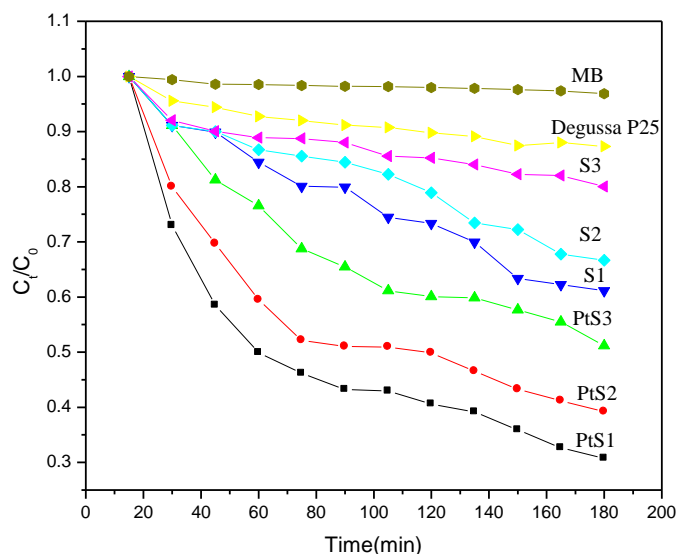
Figure 8. Photocatalytic activity of bare and platinum doped TiO_2 samples in solar light

3.7. Photocatalytic Activity

To investigate the photocatalytic activity of synthesized TiO_2 samples in solar light, the degradation of methylene blue was studied in presence of bare and platinum doped TiO_2 nanoparticles under sunlight. For comparison, photocatalytic studies were also performed with commercially available photocatalyst, Degussa P25 and the results are depicted in Fig. 8.

Methylene blue (MB) shows a maximum absorption at 661 nm. The absorption peak gradually diminishes upon solar light irradiation, illustrating the methylene blue degradation. It is clear that the anatase titania nanocubes (S1) shows higher photocatalytic activity than the other two rutile nanostructures (S2 and S3) [25]. The difference in activity of the synthesized samples is related to their surface area, particle size and phase. Small crystallite size and mesoporous texture produces high surface area TiO_2 and hence can provide more active sites and adsorb more reactive species. Since S1 is purely anatase phase and has the highest surface area among the three samples, it exhibits the highest photocatalytic activity. The appreciable activity observed for the nanorods (34 m^2 g^{-1}) compared to Degussa P25 (50 m^2 g^{-1}) is due to the preferentially grown 110 planes in the nanorod morphology [25]. The activity of different samples in sunlight is in the order PtS1> PtS2 > PtS3 >S1 > S2 >S3 > Degussa P25. The high photocatalytic activity of platinum doped TiO_2 samples compared to bare titania is mainly attributed to the decrease in band gap so that visible light is enough to excite electron from valence band to conduction band. In our investigation, we have adopted a new strategy in which nanotitania was synthesized by microwave irradiation followed by Pt loading using metal sol approach. The photo catalytic activity of platinum doped TiO_2 obtained by this approach was compared with nanotitania synthesized by hydrothermal method followed by platinum loading by metal sol method. The photo catalytic activity of $PtTiO_2$ synthesized using microwave initiated nanotitania synthesis was always found to have a higher photo catalytic activity.

IV.   Conclusions

Anatase nanocubes (S1), rutile nanospheres (S2) and nanorods (S3) were synthesized using microwave irradiation technique by changing the pH of the media. The synthesized nanostructures were doped with platinum in order to improve the photocatalytic activity of the samples under visible region. Structural and physicochemical characterization revealed the dependence of photocatalytic activity of nanotitania on different morphologies. Among bare samples anatase nanocubes (S1) exhibit a much higher BET specific surface area than rutile nanospheres (S2) and nanorods (S3). The band gap energy for anatase nanocubes is greater than that of the rutile nanospheres (S2) and nanorods (S3). Loading of platinum particles could improve the photocatalytic properties of the nanotitania under sunlight. Among the various nanotitania, Pt-doped titania

nanocubes exhibit enhanced photocatalytic activity compared to Pt-doped titania nanospheres and nanorods. Irrespective of the morphology, titania nanocubes, nanospheres and nanorods showed improved photocatalytic activity compared with commercial Degussa P25 TiO_2 photocatalyst in the degradation of the dye, methylene blue in aqueous solution under solar light irradiation.

Acknowledgements

References

[1] C-W. Hsu, C-R. Ke, Li-C. Chen, P. Chen, and J-M Ting, Effects of microwave condition on the formation and characteristics of TiO_2 submicron-sized beads and its use in all-plastic flexible dye-sensitized solar cells, Solar Energy Materials and Solar Cells, 144, 2016, 7-13.

[2] H. Jiang, Y. Liu, S. Zang, J. Li, and H. Wang, Microwave-assisted hydrothermal synthesis of Nd, N, and P tri-doped TiO_2 from $TiCl_4$ hydrolysis and synergetic mechanism for enhanced photoactivity under simulated sunlight irradiation, Chemical Engineering Journal, 274, 2015, 102-112.

[3] Yi-C. Lai, Ya-F. Wang, Y. I. Tsai, and C. -H. Tsai, A simple process for synthesizing nano Pt- and/or N-doped titanium dioxide powders by microwave plasma torch, Journal of Alloys and Compounds, 617, 2014, 834-840.

[4] X.Liu, L. Pan, T. Lv, and Z. Sun, CdS sensitized TiO_2 film for photocatalytic reduction of Cr (VI) by microwave-assisted chemical bath deposition method, Journal of Alloys and Compounds, 583, 2014, 390-395.

[5] M. Lancaster, Green Chemistry: An Introductory (Text RSC Editions: Cambridge, 2002).

[6] M. Poliakoff, J. M. Fitzpatrick, T. R. Farren and Anastas, P. T. Green chemistry: science and politics of change, Science, 297 (5582), 2002, 807-810.

[7] V. Polshettiwar, R. Luque, A. Fihri, H. Zhu, M. Bouhrara, and J. M. Basset, Magnetically Recoverable Nanocatalysts, Chemical Reviews, 111 (5) 2011, 3036–3075.

[8] V. Polshettiwar and R. S. Varma, "Microwave-assisted organic synthesis and transformations using benign reaction media", Accounts of Chemical Research, 41 (5), 2008, 629-639.

[9] M. Benaglia, Recoverable and Recyclable Catalysts (John Wiley & Sons: Chichester, 2009).

[10] S. Wittmann, A. Sh€atz, R. N. Grass, W. J. Stark, and O. A. Reiser, Recyclable Nanoparticle-Supported Palladium Catalyst for the Hydroxy carbonylation of Aryl Halides in Water, Angewandte Chemie International Edition. 49 (10), 2010, 1867–1870.

[11] C. Coperet, M. Chabanas, R. P. Saint-Arroman, and J. M. Basset, Homogeneous and Heterogeneous Catalysis: Bridging the Gap through Surface Organometallic Chemistry, Angewandte Chemie International Edition, 42 (2), 2003, 156–181.

[12] J-M. Basset, C. Coperet, D. Soulivong, M. Taoufik, and J. T. Cazat, Metathesis of Alkanes and Related Reactions, Accounts of Chemical Research, 43 (2), 2010, 323-334.

[13] T. Ibusuki, and K. Takeuchi, Removal of low concentration nitrogen oxides through photoassisted heterogeneous catalysis, Journal of Molecular Catalysis, 88 (1), 1994, 93-102.

[14] I. Nakamura, N. Negishi, S. Kutsuna, T. Ihara, S. Sugihara, and K. Takeuchi, Role of oxygen vacancy in the plasma-treated TiO_2 photocatalyst with visible light activity for NO removal, Journal of Molecular Catalysis A: Chemical, 161 (1-2), 2000, 205–212.

[15] M. Anpo, and M. Takeuchi, The design and development of highly reactive titanium oxide photocatalysts operating under visible light irradiation, Journal of Catalysis, 216 (1-2), 2003, 505-516.

[16] H. Yamashita, and M. Anpo, Application of an ion beam technique for the design of visible light-sensitive, highly efficient and highly selective photocatalysts: ion-implantation and ionized cluster beam methods, Catalysis Surveys from Asia, 8(1), 2004, 35-45.

[17] H. Kisch, and W. Macyk, Visible-light photocatalysis by modified titania, Chem. Phy.s Chem., 3(5), 2002, 399-400.

[18] M. Yamauchi, R. Abe, T. Tsukuda, K. Kato, and M. Takata, Highly Selective Ammonia Synthesis from Nitrate with Photocatalytically Generated Hydrogen on CuPd/TiO_2, Journal of the American Chemical Society,133 (5), 2011, 1150–1152.

[19] F. B. Li, X. Z. Li, M. F. Hou, K. W. Cheah, and W. C. H. Choy, Enhanced photocatalytic activity of Ce^{3+}–TiO_2 for 2-mercaptobenzothiazole degradation in aqueous suspension for odour control, Applied Catalysis A: General, 285 (1-2), 2005, 181-189.

[20] S. F. Chen, J. P. Li, K. Qian, W. P. Xu, Y. Lu, W. X. Huang, and S. H. Yu, Large scale photochemical synthesis of M@TiO_2 nanocomposites (M = Ag, Pd, Au, Pt) and their optical properties, CO oxidation performance, and antibacterial effect, Nano Research, 3 (4), 2010, 244-255.

[21] L. Han, Y. Xin, H. Liu, X. Ma, and G. Tang, Photoelectrocatalytic properties of nitrogen doped TiO_2/Ti photoelectrode prepared by plasma based ion implantation under visible light, Journal of Hazardous Materials,175 (1-3), 2010, 524-531.

[22] W. T. Sun, Y. Yu, H. Y. Pan, X. F. Gao, Q. Chen, and L. M. Peng, CdS Quantum Dots Sensitized TiO_2 Nanotube-Array Photoelectrodes, Journal of the American Chemical Society, 130 (4), 2008, 1124-1125.

[23] J. Thomas, K. P. Kumar, and S. Mathew, Hydrothermal Synthesis of Samarium Doped Nanotitania as Highly Efficient Solar Photocatalyst, Science of Advanced Materials, 2 (4), 2010, 481–488.

[24] T. Suprabha, H. G. Roy, J. Thomas, K. P. Kumar, and S. Mathew, Microwave-Assisted Synthesis of Titania Nanocubes, Nanospheres and Nanorods for Photocatalytic Dye Degradation, Nanoscale Research Letters, 4 (2), 2009, 144–152.

[25] T. Suprabha, H. G. Roy, and S. Mathew, Gold Doped Nanotitania-Synthesis, Characterization and Morphology Dependence on Photocatalysis, Science of Advanced Materials, 2 (1), 2010, 107-114.

[26] T.Suprabha, H. G. Roy, and S. Mathew, Silver Loaded Titania Nanostructures with Extended Spectral Response for Enhanced Solar Photocatalysis, Journal of Nanoscience Letters, 2, 2012, 19-26.

[27] T. Suprabha, and S. Mathew, Influence of Palladium loading on the degradation property of Titania Nanostructures, JOSR Journal of Applied Chemistry (JOSR-JAC), 2014, 41-50.

[28]   J. D. Grunwaldt, C. Kiener, C. Wogerbauer, and A. Baiker, Preparation of Supported Gold Catalysts for Low-Temperature CO Oxidation via Size-Controlled Gold Colloids, Journal of Catalysis, 181 (2), 1999, 223-232.

[29]   D Zhang, D Yang, H Zhang, C Lu, and L Qi , Synthesis and photocatalytic properties of hollow microparticles of titania and titania/carbon composites templated by Sephadex G-100, Chemistry of materials, 18 (15), 2006 3477–3485.

[30]   S. Chavadej, P Phuaphromyod, E Gulari, and P Rangsunvigit, Photocatalytic degradation of 2-propanol by using Pt/TiO 2 prepared by microemulsion technique, Chemical Engineering , 137 (3), 2008, 489–495

[31]   N. Sobana, M. Muruganadham, and M.Swaminathan, Nano-Ag particles doped TiO$_2$ for efficient photodegradation of Direct azo dyes. J Mol Catal A 258, 2006, 124-132.

[32]   D. Z. Li, Z. X. Chen, Y. L. Chen, W. J. Li, H. J. Huang, X. Z. He, and Y. H. Fu, A new route for degradation of volatile organic compounds under visible light: using the bifunctional photocatalyst Pt/TiO$_2$−xNx in H$_2$–O$_2$ atmosphere. Environ. Sci. Technol. 42, 2008, 2130–2135.

[33]   N. Zhang, S. Liu, X .Fu, and Y. J. Xu , Synthesis of M@ TiO$_2$ (M= Au, Pd, Pt) core–shell nanocomposites with tunable photoreactivity, The Journal of Physical Chemistry C, 115 (18), 2011, 9136–9145.

[34]   Y. Cong, J. Zhang , F. Chen , M. Anpo, and D. He, Preparation, Photocatalytic Activity, and Mechanism of Nano-TiO$_2$ Co-Doped with Nitrogen and Iron (III), . **J** Phys Chem 28, 2007, 10618-10623.

[35]   X. Chen and S. S. Mao, Titanium dioxide nanomaterials: synthesis, properties, modifications, and applications. Chem Rev 107, 2007, 2891-2959.

[36]   I. Burlacov, J. Jirkovský, M. Müller, and R.B. Heimann, Induction plasma-sprayed photocatalytically active titania coatings and their characterisation by micro- Raman spectroscopy, Surface & Coatings Technology 201, 2006, 255–264.

[37]   S. J. Rigbya, A. H. R. Al-Obaidi, S. K. Lee, D. M. Stay, and P. K.Robertson The application of Raman and anti-stokes Raman spectroscopy for in situ monitoring of structural changes in laser irradiated titanium dioxide materials, J Appl Surf Sci 252, 2006, 7948-7952.

[38]   W. Song , Y. Wang, and B. Zhao, Surface-Enhanced Raman Scattering of 4- Mercaptopyridine on the Surface of TiO$_2$ Nanofibers Coated with Ag Nanoparticles. J Phys Chem C 111; 2007, 12786-12791.

[39]   M. Kerker, and C. G. Blatchford, Elastic Scattering and Absorption, and Surface-enhanced Raman Scattering by Concentric Spheres Comprised of A Metallic and Dielectric Region, J Phys Rev B 26, 1982, 4052-4063.

[40]   W. Liping, L.Baoshun, L.Chao, Z, and Z. Xiujian , Preparation, Characterization and Photocatalytic,Property of Ag-loaded TiO$_2$ Powders Using Photodeposition Method, Journal of Wuhan University of Technology-Mater Sci Ed 24; 2009, 258-2

[41]   D. Regonini, A. Jaroenworaluck, R. Stevensa, and C. R. Bowen , Effect of heat treatment on the properties and structure of TiO$_2$ nanotubes: phase composition and chemical composition., Surf Interface Anal. 42, 2010, 139–144.